Laboratory tests on HeNOS, the MCAO test bench for NFIRAOS

Matthias Rosensteiner[a]*, Paolo Turri[b], Jean-Pierre Veran[a], David Andersen[a], Paolo Spano[c] and Glen Herriot[a]

[a] NRC Herzberg - Astronomy and Astrophysics
[b] University of Victoria
[c] INAF - Instituto Nazionale di Astrofisica

Abstract

HeNOS is a test bench designed to be a scaled down version of NFIRAOS, the first light MCAO instrument for the Thirty Meter Telescope. The system was designed and built in the adaptive optics lab at NRC Herzberg in Victoria. The goal of the test bench is to assess the prediction quality of MAOS, the simulation software for NFIRAOS, to test the robustness of the tomographic algorithm under slowly changing conditions and to evaluate the calibration methods considered for the real instrument. For these tasks it is important to know the real dimensions of HeNOS with good precision. The goal of the tests presented here is to obtain the system parameters from the bench and compare them to the design.

1 Original design

The plan for the HeNOS MCAO test bench is to simulate an 8 m telescope. This gives us for our ground deformable mirror with 97 actuators with 0.9 meters roughly the same actuator spacing as it will be available in NFIRAOS. The science camera is designed with an 10.9 arcsec field of view, using a 2448x2048 CCD. The wavelength of the NGS, as well as the LGS, is 670 nm and there should be sufficient stars in the FoV to have a good evaluation of the performance, while the LGS asterism is a square with a side length of 4.5". The wavefront sensor has 30 subapertures across the pupil, which gives an oversampling of the deformable mirror. The atmosphere we like to correct for should have an r_0 of 0.75 m, devided into three layers at 0 km, 4.2 km and 14 km, with a relative strength of 72.3%, 19.8% and 7.9%. The high altitude deformable mirror is conjugated to the height of 11.2 km. In order to keep the degradation of the correction over the field of view similar to NFIRAOS, we stretch all altitudes on the bench with a factor of 11.

The bench was built with this design in mind, more details can be found in [2, 1]. The task of this report is to obtain the precise parameters, which might slightly deviate but should be close to this prescription. In the evaluation it is necessary to fix one factor, from which all other ones are derived. We chose the asterism size of the LGS as fixed. The reason is that the LGS are solid holes in a plate, which are very stable and unlikely to change. All other parameters are determined based on that.

*Corresponding author: matthias.rosensteiner@nrc-cnrc.gc.ca

2 Wavefront sensor camera plate scale

The first parameter we compute is the pixel size of the wavefront sensor. This can be relatively easily obtained, as we use a single lenslet array for the four wavefront sensors, where each lenslet images the whole LGS asterism. For each lenslet we compute the size of the asterism and derive the plate scale of the wavefront sensor.

The algorithm to determine the pixel scale consists of several steps:

1. Identification of the stars, and therefore illuminated subapertures, in the images
2. Placement of the stars on the wavefront sensor grid
3. Determination of the distances between the stars for each subaperture

With help of this method we calculate for the LGS asterism an average side length of 20.58 (+/- 0.51) pixels on the detector. Therefore, the pixel size of the wavefront sensor is 1.06 μradians.

In a second test we look at the spacial variations of the asterism size over the wavefront sensor. In Figure 1 we plot the asterism size in each subaperture. This shows clearly that there is a significant variation of the size over the whole field with the smallest scale approximately in the center. This indicates that there is some plate scale distortion in the wavefront sensor path of our system.

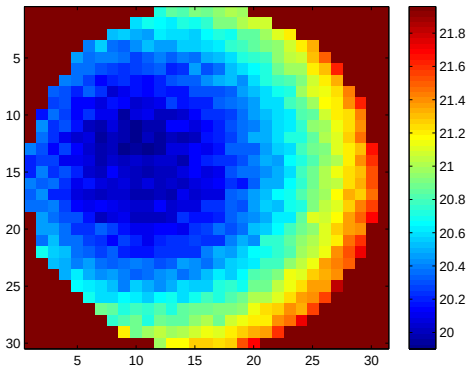

Figure 1: Asterism size over the wavefront sensor camera

3 Science camera plate scale

The LGS asterism is also useful to determine the science plate scale as we can see the defocused LGS spots in the camera. The image of the LGS asterism is shown in Figure 2. We estimate the centers of these blobs and use them to derive the plate scale of the science camera. From the 4.5" asterism we obtain a pixel scale of 3.46 mas, or 16.8 nradians. This is close to the design and gives us a FoV of 11.04. Note that the ghosts visible in the image are due to the double reflection between the deformable mirrors.

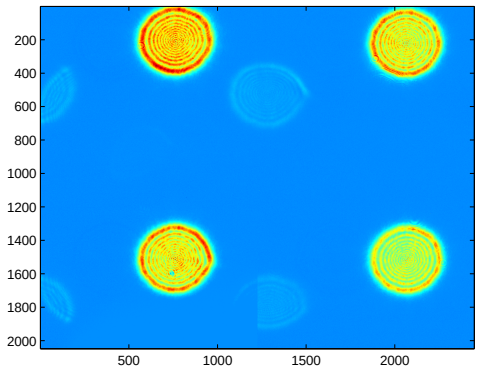

Figure 2: Science camera image of the LGS asterism

Another method to estimate the plate scale is to use a tilt, measured on the wavefront sensor and the science camera. Those values give the relation between the two plate scales. The result was similar, but due to the large difference in the plate scales the noise in that measurement was higher than with the method described first.

4 NGS asterism size and distortions

After the determination of the plate scale of the science camera, we obtain the size of the NGS asterism on sky. The asterism is created with a lenslet array, which gives a uniform grid over the whole science camera. The advantage of this is that in later tests we will be able to determine the performance of our system for a good number of positions in the field of view. With a fit of a uniform grid we can also look at field distortions.

We identify the stars in the images with the same algorithm as for the wavefront sensor plate scale determination and obtain the precise location with a center of gravity estimation. The stars are placed on a grid, as in the case of the wavefront sensor. From the grid we can easily compute the distance between two neighboring stars. The average over all these distances is computed.

The computation of the distance between two neighboring stars in the grid gives an average separation of 121.1 (+/-0.4) pixels. Including the plate scale of the science camera, this corresponds to an asterism size of 419 mas star separation.

When we look at the field distortions in Figure 3, no well-known distortion can be seen. An even better method to identify the NGS asterism and the science field distortions might be the use of self-referencing techniques.

As a side test, we can perform the same distortion estimation for the wavefront sensor geometry. This is done for each guide star separately. The results in Figure 4 shows a uniform focus distortion for all guide stars.

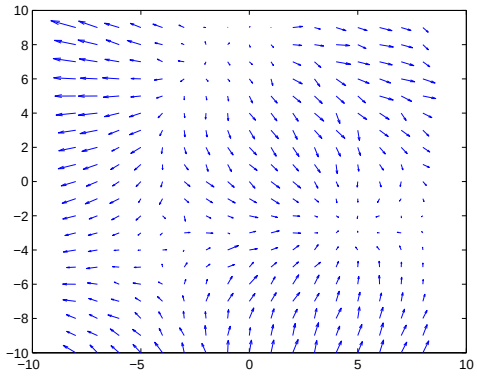

Figure 3: Field distortion on the science camera (max. 4 pixel arrows)

5 Telescope size

On the bench, the aperture of the telescope is initially defined by an iris of 10 mm of diameter. Its size "on sky" can be measured by the diameter of the first Airy ring of the science images. Using a 10 mm stop the ring is too small, because of alignment aberrations, making it difficult to obtain a correct detection; by reducing the iris to 3 mm, the first ring is distant enough from the core while keeping a sufficiently bright aperture.

Stars are first identified on the image in the same way as for the measurement of the plate scale computation. A stacked image of all the NGSs has a higher S/N than the individual ones and is created by superimposing their images with their brightest pixel aligned. The first Airy ring is isolated in the image by cutting a ring comprised between the first and second zero of the Airy disk defined, respectively, at $1.22\lambda/D$ and $2.23\lambda/D$ (Figure 5). To measure the diameter of the ring, its image is linearized by a transformation from polar to Cartesian coordinates. For each column of the transformed image the radial centroid is found, representing the distance of a section of the ring from the center. The radius r_1 of the ring is measured by the median of these centroids, then the aperture diameter is calculated from the equation for the first Airy ring $r_1 = 1.64\lambda/D$.

A stop of 3 mm on in the telescope collimated space of the bench represents on sky an aperture of 2.44 m, that correspond to 8.13 m for a 10 mm iris, as from the design.

6 Wavefront sensor characteristics

The design of HeNOS predicts about 30 subapertures over the pupil of the telescope, a number that should be determined precisely.

The algorithm to determine the subaperture size of the wavefront sensor consists of several steps:

1. Identification of the wavefront sensor
2. Calculation of the illumination of the subapertures
3. Determination of the size and location of the pupil

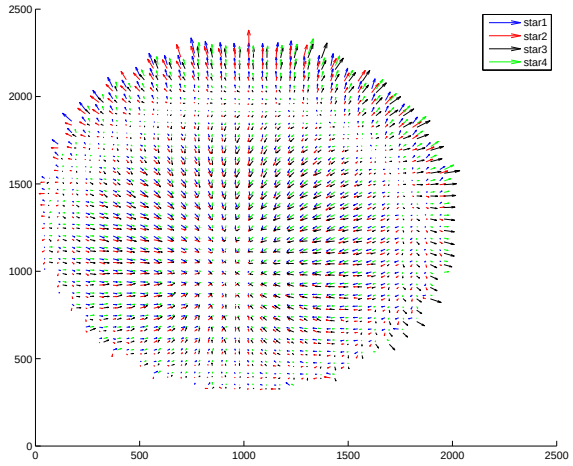

Figure 4: Field distortion on the wavefront sensor camera

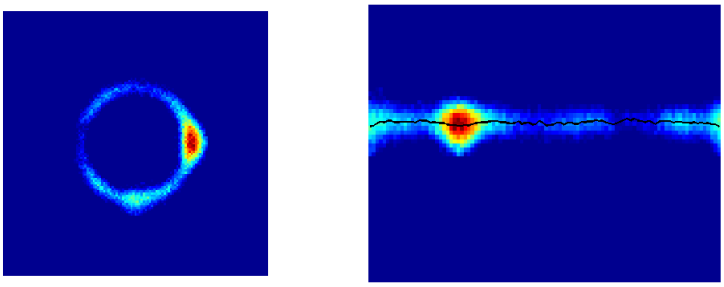

Figure 5: First Airy ring of the stacked NGSs & polar transformed

We obtain the geometry of the inner, illuminated subapertures with the same method as for the determination of the wavefront sensor plate scale. With the help of a fitted grid we can define subapertures outside the illuminated zone, which still might contain some flux at the boundary. The illumination of each subaperture is the sum of all pixel values in the subaperture area.

To determine the pupil size, the measured illumination pattern is matched to a modeled illumination pattern, which can be adjusted with respect to radius and center location. The artificial illumination pattern uses a circle as geometric description of the pupil, the value for each subaperture in these patterns are determined by the percentage of coverage.

The first step of the pupil identification is the computation of the illumination pattern. This is done for each of the four wavefront sensors separately. In Figure 7 the illumination for one wavefront sensor is shown.

The optimization method gives for the radius of the pupil 15.226 (+/- 0.016) subapertures, which leads with a telescope diameter of 8.13 m to an estimated subaperture size of 0.267 m.

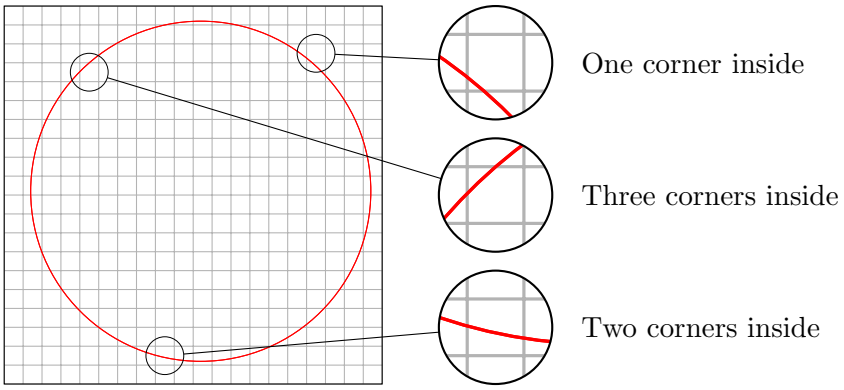

Figure 6: Example wavefront sensor grid with illumination pattern

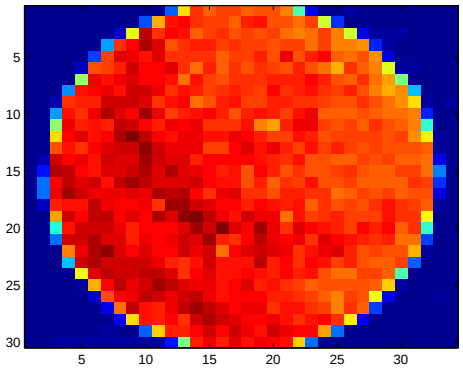

Figure 7: Illumination of one wavefront sensor

7 Deformable mirror characteristics

The system has two deformable mirrors, which are conjugated to different altitudes. We determine the actuator spacing and the altitude conjugation of the mirrors, which has an impact on the correction quality. Additionally, we can evaluate how well the mirrors are aligned with respect to the pupil stop. The basis for this experiment is the poke matrices of the system, that means a poke matrix for each deformable mirror to wavefront sensor combination.

In the first step for each deformable mirror the relation with each wavefront sensor is determined. That means we calculate where the actuators are located in the wavefront sensor geometry. This data is then used to obtain the actuator spacing and the conjugation altitude as well as the error in the centering of the mirrors with a least squares fit. The error in the center is used to align the mirrors better to avoid vignetting of the pupil.

From the scaling of the fit of the ground conjugated deformable mirror we can derive the actuator spacing of the mirrors. Knowing that the LGS asterism is a square with a size of 4.5 arcsec, the conjugation height of the high altitude mirror is estimated from the shear of the metapupils.

From the poke matrix the relations between the wavefront sensors and the deformable mirrors are established. In Figure 8 we can see an example mapping of the ground deformable mirror onto one wavefront sensor. The pupil is marked by the blue circle, the blue crosses are the calculated actuator positions, trusted positions, that are used for the fitting, have an additional red circle. In pink is the fitted alignment of the deformable mirror. This shows that the error between the trusted positions and the fitted locations is small.

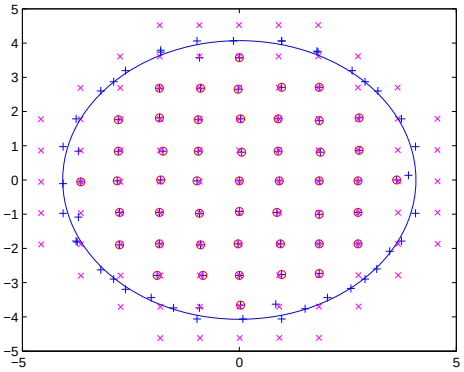

Figure 8: Estimated position of the ground deformable mirror with respect to one wavefront sensor (blue: actuator positions, red: trusted actuators, pink: fitted dm)

From the fitting the actuator distance can be estimated as 0.914 m. The calculation of the altitude gives a conjugation to 12 km, which is slightly above the design.

8 Turbulence phase screens properties

In this section are determined the phase screen characteristics such as geometric properties (altitude and wind speed) and their turbulence power. The first part requires simple measurements of distances and sizes on the bench, while for the second we need to observe the effects of turbulence on both the science and the WFS cameras.

For each phase screen the distance of the optical axis to the rotation center is measured. The link to the real dimensions is provided by the relation between the size of the telescope, measured to be 8.13 m, and the size of the pupil on the collimated spaces. This gives the relation between the rotational speed of the screens and the resulting wind speed. Note that due to the rotational movement the speed is never uniform over the metapupil.

The distance between the optical surfaces in the conjugated space of the deformable mirrors is measured. Using this and the conjugation heights of the deformable mirrors as calculated in the previous section, we find that the scale in the collimated space to transform distances on the bench to altitudes in the atmosphere is 28.22 mm/km. For the ground phase screen, the scale is the one of the DMs spaces times the square of the ratio between the sizes of the aperture (10 and 13.35 mm), that corresponds to 15.8 mm/km. Table 1 shows the phase screen circumferences and altitudes.

The turbulence power is measured for each phase screen separately. One hundred sample positions are selected across each screen to obtain good statistics of the slopes on the WFS and a smooth

Phase screen	Circumference	Altitude
Ground	295 m	0.6 km
Mid-altitude	97 m	5.2 km
High-altitude	92 m	16.3 km

Table 1: Phase screen geometric characteristics

point spread function (PSF) on the long exposure image on the science camera. Additionally, the PSF is measured without phase screens to be used as a reference.

In the science image for each star in the FoV the FWHM is computed and the Fried parameter derived, assuming Kolmogorov statistics. From the WFS slopes the phase is reconstructed using CuReD and its standard deviation used to obtain the Fried parameter in an independent way. Note that due to the cone effect of the LGS the measurements of the high altitude phase screens has to be corrected.

In Figure 9 are the four images of a star taken with the science camera before the use of phase screens and using combinations of phase screens. In Table 2 are the Fried parameters measured for the three phase screens with both the science camera and WFS, as well the nominal value used by the manufacturer. The Fried parameters measured by the WFS are larger than those from the science camera and this is reasonable considering that the WFS is blind to the highest spatial frequencies of the turbulence. The science camera measurement should therefore be preferred to the WFS one. For all the phase screens, the measurement is well within 10% of the nominal value. The relative power of the phase screens in term of $\sigma^2 \propto r_0^{-5/3}$ are 74.3%, 17.4% and 8.2%.

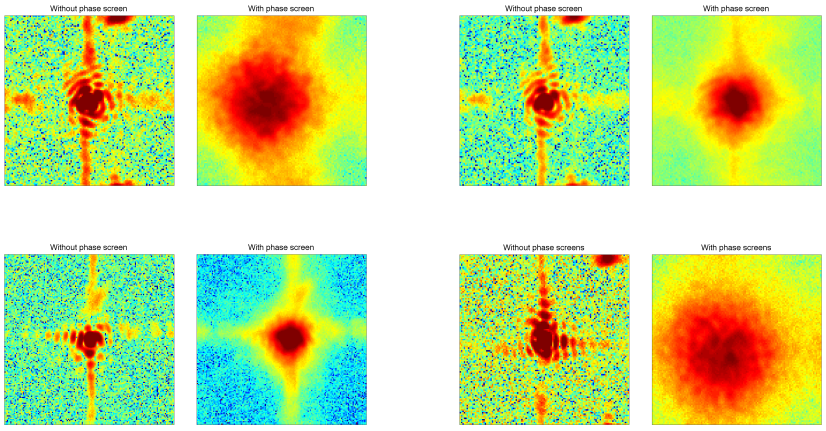

Figure 9: Science camera images of a star using different combinations of phase screens: ground on the top-left, mid-altitude on the top-right, high-altitude on the bottom-left and all of them on the bottom-right. For each case the same star is shown without the use of phase screens

Phase screen	$r_{0,SC}$ (670 nm)	$r_{0,SC}$ (500 nm)	$r_{0,WFS}$ (670 nm)	$r_{0,WFS}$ (500 nm)	r_0 (500 nm)
Ground	0.99 m	0.70 m	1.15 m	0.81 m	0.74 m
Mid-altitude	2.37 m	1.67 m	2.83 m	1.99 m	1.61 m
High-altitude	3.72 m	2.62 m	3.80 m	2.68 m	2.79 m
All	0.83 m	0.58 m			

Table 2: Fried parameters of the phase screens measured through the science camera and the WFS independently. In the last column is the nominal Fried parameter used for manufacturing.

Parameter	Design	Measurement
LGS asterism size	4.5"	4.5" (defined)
Telescope size	8 m	8.13 m
Actuator distance	0.89 m	0.914 m
Subaperture size	0.27 m	0.267 m
Science FoV	10.9"	11.04"
DM heights	[0 km, 11.2 km]	[0 km, 12 km]
r_0 (500 nm)	0.609	0.584
phase screen heights	[0 km, 4.2 km, 14 km]	[0.6 km, 5.2 km, 16.3 km]
phase screen strength	[72.3%, 19.8%, 7.9%]	[74.3%, 17.4%, 8.2%]
LGS height	90 km	98.5 km

Table 3: Summary of the measured bench parameters.

9 Summary

We summarize the dimensions we found in our calibration and compare them to the HeNOS bench design in Table 3.

In general we can claim that the bench we built is quite close to the design of our system. Additionally, the estimation methods we developed can be used to align the system to obtain a better accuracy. With these parameters we can built our error budget to a great precision. It allows us to evaluate the results of further tests in comparison to the predicted performance.

References

[1] Paolo Turri, David R. Andersen, Jean-Pierre Véran, Paolo Spanò, Matthias Rosensteiner, and Eric A. McVeigh. An MCAO test bench for NFIRAOS, 2014.

[2] Jean-Pierre Véran, Eric McWeigh, David Andersen, Carlos Correia, Glen Herriot, and John Pazder. The HIA MCAO laboratory bench , 2012.